THEORETICAL ANALYSIS OF METAL CUTTING WITH LARGE NEGATIVE RAKE CUTTING TOOLS

by

JOHN WAYNE HEIN

B.S., Kansas State University, 1977

A MASTER'S THESIS

Submitted in Partial Fulfillment of the

Requirements for the Degree

MASTER OF SCIENCE

Department of Mechanical Engineering

Kansas State University

Manhattan, Kansas

1979

Approved By:

F. C. Appl

Major Professor

ABSTRACT

An approximate slip-line field is developed for a range of negative rake angles beyond the range where ordinary metal cutting theory applies. In this range of large negative rake angles, the flow of metal along the tool is in opposite directions on either side of a stagnation point on the tool. This divided flow results in frictional stresses which are also in opposite directions. The slip-line field accounts for this complex friction distribution and is used to calculate the cutting forces and frictional stresses for various rake angles and friction coefficients.

TABLE OF CONTENTS

LIST OF TABLES

LIST OF FIGURES

LIST OF FIGURES (Continued)

NOMENCLATURE

α	Negative Rake Angle
t	Depth of Cut
U	Workpiece Velocity
U_1, U_2, U_3	Velocities in the Hodograph
U_1^*, U_2^*, U_3^*	Velocity Discontinuities in the Hodograph
F_n	Cutting Force Component Normal to the Workpiece Velocity
F_t	Cutting Force Component Tangential to the Workpiece Velocity
x	Coordinate Direction Parallel to the Workpiece Velocity
k	Yield Stress in Pure Shear
Y	Yield Stress in Pure Uniaxial Tension
σ, σ_1, σ_2, σ_n, σ_t	Normal Stresses
τ, τ_1, τ_2, τ_{xy}	Shear Stresses
p, P_1, P_2, P_3	Hydrostatic Stresses
ϕ, ϕ_2, ϕ_3	The Counter-Clockwise Angle of an α-line from the Positive x-Axis
α-line	Slip-Line of the Family Denoted by the Parameter ϕ
β-line	Slip-Line of the Family Denoted by the Parameter $(\phi + \pi/2)$
u	Velocity Parallel to an α-line
v	Velocity Parallel to a β-line
R	Fan Radius
ζ	Shear Plane Angle
θ	Stress Discontinuity Angle
P_m	Mean Pressure on the Rake Face

η_1, η_2	Friction Angles on the Upper and Lower Sections of the Tool Respectively
ℓ_1, ℓ_2	Lengths of the Upper and Lower Sections of the Tool Respectively
m	Adhesion Coefficient
μ	Friction Coefficient
A_R	Real Area of Contact
β_1, β_2	Parameters in the Equation for A_R
ξ	Parameter in the Equation for $\left(\frac{\sigma_n}{2k}\right)_{lim}$

INTRODUCTION

Metal cutting is a very important process in industry, yet the mechanics of it are not completely understood. Much research has been done in the area of metal cutting to try to predict how chips form and what forces are required to produce them. It is also hoped that learning more about the metal cutting process will lead to a better understanding of the friction between the tool and the workpiece and thus shed more light on the related problem of tool wear.

Merchant [1], [2], [3] was about the first to study the problem of metal cutting analytically. His work was based on the assumption of a perfectly sharp tool and a single shear plane. But actually cutting tools are not perfectly sharp. The tip of a cutting tool is rounded and the material flow around the tip is very complex because the effective rake angle is not constant around the tool tip.

Albrecht [4] studied the force due to a rounded tool tip and called it the ploughing force. This new force allowed for the construction of a more detailed force diagram which was a step towards a better analytical solution to the metal cutting process.

A major problem in analyzing the ploughing force and the material flow around the tool tip is that the effective rake angle varies around the tool tip from a positive angle at the face of the tool through the negative range to essentially -90° at the tool tip. The difficulty is that the stresses and flow patterns of large negative rake cutting are unknown. Since Merchant's model for metal cutting does not hold for large negative rakes, the problem is still unsolved.

In ordinary metal cutting the tool tip radius is small compared to the undeformed chip thickness. However, there are many important cutting situations in which the tool tip radius is large compared to the undeformed chip thickness such as in metal grinding [5] or in rock cutting with diamond cutting tools [6]. In these cases the cutting force may be predominantly a ploughing force and it becomes important to know the stresses and flow characteristics around the tool tip.

Rubenstein, et al [8] conducted cutting tests using single diamond grains and high speed steel tools to simulate the cutting action of a single abrasive grit in a grinding process. They found a critical angle, at which the chip ceases to form and pure ploughing begins, to be about -55°. From these experiments they developed a new model for the metal flow around the rounded portion of the tool tip [9]. Their model included a stagnation point on the tool tip located where the effective rake angle was equal to the critical rake angle. Above this stagnation point the material would flow up as part of the chip and below the point the material would flow down under the tool.

Rowe and Wetton [10] developed slip-line fields for a truncated conical tool. Their work indicated how a bulge could form in front and at the sides of the tool, and they were able to predict the transition from a bulge to a chip. Komanduri [11] conducted experiments with negative rake tools and was able to obtain chips with rake angles down to -75° when cutting steel. Below 75° negative rake, no chips were formed but the side flow of the metal was considerably increased. Komanduri suggested that there is a stagnation point on the tool face above which material flows up the tool face and below which the material flows under the tool. The location of the stagnation point depends on the rake angle.

Lal and Shaw [12] conducted experiments with a hard spherical ball. The sphere was scraped across various materials. They observed a steady-state piling-up of material in front of the ball for small depths of penetration. As penetration was increased to some critical depth, in relation to the diameter of the ball, chips were formed.

Abdelmoneim and Scrutton [13] analyzed orthogonal cutting with round nosed tools in which the depth of cut was less than the tool nose radius. They assumed there was a stable build-up of material on the tool tip below the critical rake angle.

Sakamoto and Tsukizoe [14] conducted scratch tests on copper using conical diamonds. In their work they obtained an excellent series of optical micrographs which show a prow forming in front of the diamond cone. As the sliding distance was increased, the prow gradually grew until a chip was formed. They found that for sufficiently large negative rake angles, all of the material was displaced around the front and sides of the cone but no chips were formed.

From this brief review of the literature it appears there is still much uncertainty in the theory of negative rake metal cutting. A major reason for this uncertainty and one of the most difficult facets of the problem is that the boundary conditions of the problem are not completely known a priori. When a rake angle is specified, the direction of chip flow is known, but the size and shape of the chip and deformation zone remain unknown. Hill [20] suggested that there may not be a unique steady-state solution of the single shear-plane type. He used a method of eliminating the configurations in which the material was overstressed to obtain a range of possible solutions. The real solution for a given problem would then lie in the range of possible solutions and would depend on the initial conditions.

Experimental results obtained by Ramalingam and Hazra [21] suggest that additional constraints on the metal cutting problem must come from the structure and properties of the work material. They suggested that the constancy of dynamic shear stress plays a dominant role in determining the geometry of the cutting process. However they were not able to determine the exact role of the dynamic shear stress. They concluded that the geometric configuration of the problem could not be fully defined knowing only the chip flow direction and the dynamic shear stress, and that an additional constraint is necessary to determine the overall configuration of the process.

When the process of large negative rake metal cutting is considered, another major problem is encountered in addition to the unknown geometry. Most experimental work with negative rake angles indicates a stagnation point on the tool face. The location of the stagnation point for various cutting conditions is far from being clearly understood. The presence of a stagnation point on the tool face indicates that the work material is flowing in opposite directions on either side of the stagnation point. This results in the friction on the tool being in opposite directions across the stagnation point which results in a complex force distribution on the tool. Similarly the shear stress distribution in the material near the tool is also more complex.

DESCRIPTION OF THE PROBLEM

This study was undertaken to develop an improved theoretical model of orthogonal metal cutting with large negative rake tools. It was desired to learn more about the flow of the material in the vicinity of the tool as well as the stresses and forces involved in the process. The basic problem is shown in Figures 1 and 2.

Most metal cutting applications are actually a three-dimensional process but many can be idealized as two-dimensional without significant loss of accuracy. In this study the problem will be considered a two-dimensional plane strain problem. The tool is rigid and stationary with a straight cutting surface of unit width. The negative rake angle is α and the depth of cut is t as shown in Figure 2. The workpiece is a rigid-perfectly plastic material moving towards the tool with a velocity U. Work hardening of the material as well as temperature effects will be neglected. The plastic zone shown in Figure 1 is the region of the workpiece which has yielded according to the von Mises yield criterion. The remainder of the workpiece outside the plastic zone is rigid. The chip shown in Figure 1 is assumed to be stress free and thus exerts no force on the cutting tool.

The forces F_n and F_t shown in Figure 2 are the normal and tangential components of the cutting force. It is desired to obtain an upper bound for the cutting force components as functions of rake angle, depth of cut, and material properties.

The governing partial differential equations for two-dimensional flow of a rigid-plastic material are well known, but there are no straight forward approximate procedures to solve this type of boundary value problem,

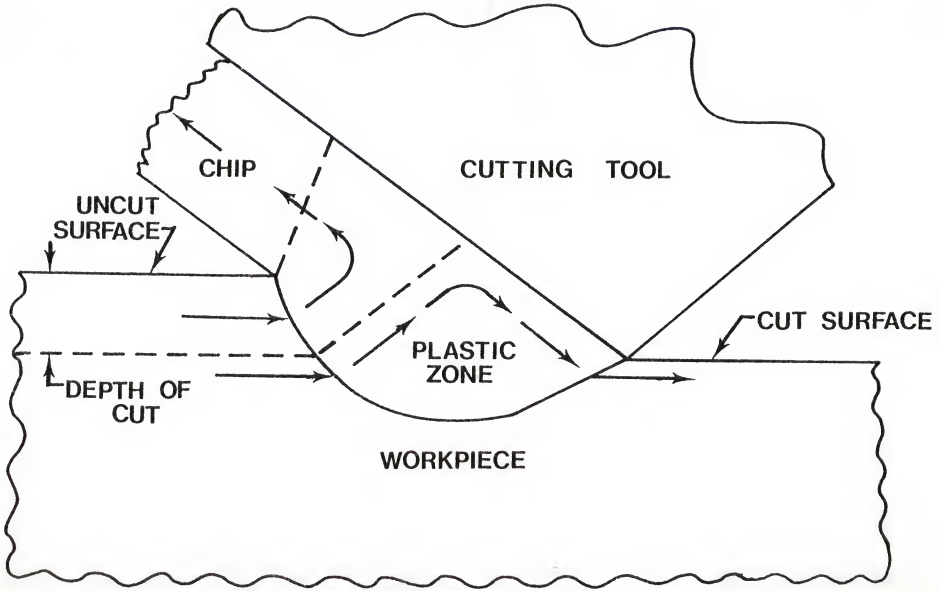

Figure 1

Schematic of Cutting with a Large Negative Rake Tool

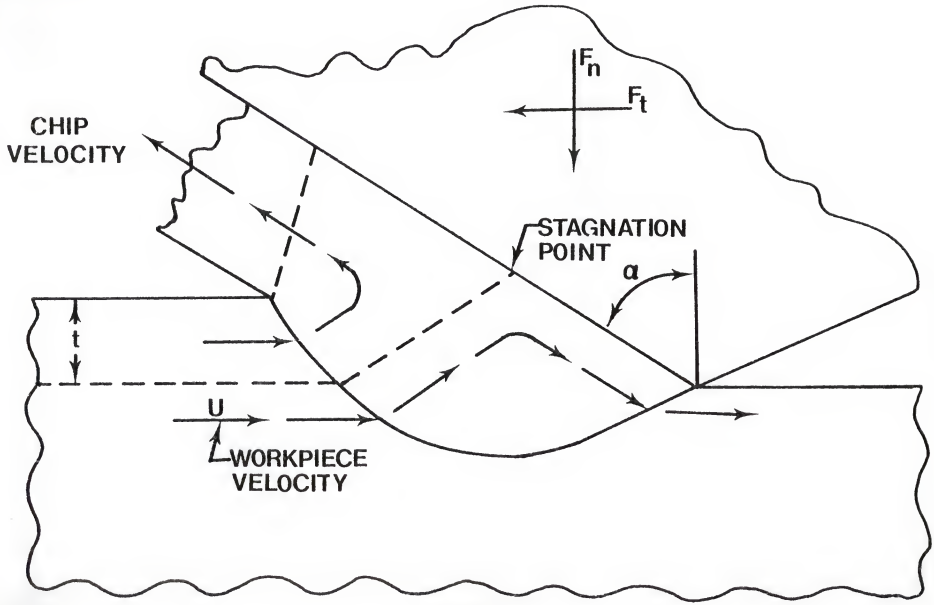

Figure 2

Schematic of Cutting with a
Large Negative Rake Tool

particularly when the shape of part of the boundary is not known a priori. The general nature of solutions is however revealed in terms of the characteristics of the differential equations which are designated as slip-lines. Considerable intuition is required to use the slip-line method to solve problems in which the shape of part of the boundary is unknown. The quality of results obtained by the slip-line method is somewhat dependent on the intuition of the investigator since the procedure of obtaining a solution is not straight forward. However, the slip-line method is well suited to the problem of negative rake metal cutting and will be used here.

In many processes such as extrusion and sheet drawing the boundaries are known and the slip-line theory can be applied directly to obtain an upper bound solution. However since the boundaries for the metal cutting problem are not known a priori the slip-line method results in a trial and error process. A slip-line field can be constructed assuming a set of boundaries based on intuition or observation of experimental work. Then a valid velocity field (hodograph) must be found corresponding to the slip-line field. If a valid hodograph cannot be found a new slip-line field must be constructed. The process is repeated until a slip-line field with a corresponding valid hodograph can be found. If the slip-line field satisfies all of the requirements of the slip-line theory, it is an upper bound solution to the problem. This trial and error procedure with unknown boundaries and two-way flow makes the process of solving the large negative rake cutting problem very complex.

SLIP-LINE THEORY

The slip-line method is a practical method of solution for certain plane plastic flow problems. The method is based on several simplifying assumptions which are reasonably valid for the problem of large negative rake metal cutting.

A plane flow problem is one in which the velocity of the material is always parallel to a given plane, say the (x,y) plane. Thus, the velocity and all material properties are functions of x and y but do not vary with the third coordinate direction. This assumption is reasonable for large negative rake metal cutting when the depth of cut is small compared to the width of the tool.

The work material is assumed to be a rigid-perfectly plastic solid. This means that the material is rigid and has infinite elastic moduli under any state of stress below the yield stress of the material. When the material is stressed above the yield stress it behaves plastically. This assumption is valid for problems in which the material is not highly constrained, in which case, the elastic strains are small compared to the plastic strains. In the problem of large negative rake cutting the material is not highly constrained and hence the assumption of rigid-plastic material behavior is valid.

The von Mises yield criterion is commonly used in plasticity. According to this theory the material yields plastically when the shear stress in the material reaches the pure shear yield stress (k). This is easily visualized on a Mohr's circle as the condition of stress in which the radius of the circle is equal to k. The shear stress in a perfectly

plastic material never exceeds k. According to the von Mises yield criterion the pure shear yield stress is equal to the yield stress for pure uniaxial tension divided by $\sqrt{3}$. From this yield criterion the following yield equation is obtained.

$$\frac{\sigma_x^2 - \sigma_y^2}{2} + \tau_{xy}^2 = k^2 \tag{1}$$

There are three unknown stresses σ_x, σ_y, and τ_{xy}. Compressive stresses are considered negative and tensile stresses positive. To solve for these unknown stresses two more equations are necessary. These are the equilibrium equations of plane stress which are given below.

$$\frac{\partial \sigma_x}{\partial x} + \frac{\partial \tau_{xy}}{\partial y} = 0 \tag{2}$$

$$\frac{\partial \tau_{xy}}{\partial x} + \frac{\partial \sigma_y}{\partial y} = 0 \tag{3}$$

There are now three equations for the three unknown stresses. There are also two velocity equations which must be satisfied throughout a plastically deforming region. The first is the continuity equation (4) in which v_x and v_y are the components of velocity in the x and y directions respectively.

$$\frac{\partial v_x}{\partial x} + \frac{\partial v_y}{\partial y} = 0 \tag{4}$$

The second velocity equation is the isotropy equation (5) which is obtained from the assumption that for an isotropic rigid-plastic material the principal axes of stress and strain rate coincide.

$$\frac{\partial v_x}{\partial y} + \frac{\partial v_y}{\partial x} = -\left[\frac{\partial v_x}{\partial x} - \frac{\partial v_y}{\partial y}\right] \cot 2\phi \tag{5}$$

The angle ϕ in equation (5) is defined such that $(\phi + \frac{\pi}{4})$ is the counterclockwise rotation of the direction of the algebraically greatest principal stress from the positive x axis.

It now appears that for a problem with given boundary conditions there are enough equations to theoretically solve for the stresses and velocities exactly. In general, however, problems of plane plastic flow are statically indeterminate and cannot be solved exactly. This is the case for the problem of large negative rake metal cutting and hence an approximate technique must be used to obtain a solution.

The slip-line method is a semi-graphical approximate technique involving the method of characteristics. A slip-line field which satisfies the stress equations can be constructed graphically. The Hencky equations which result from applying the method of characteristics to the stress equations are used to calculate stresses along the slip-lines. Similarly a velocity diagram or hodograph can be constructed which satisfies the velocity equations. The Geiringer equations which are obtained by applying the method of characteristics to the velocity equations can be used to calculate velocities in the slip-line field. However, in many cases velocity values obtained graphically from the hodograph are sufficient.

The hydrostatic stress p must be introduced to obtain the Hencky equations.

$$p = -\tfrac{1}{2} (\sigma x + \sigma y) \tag{6}$$

For a material in the plastic state, p is the normal stress coordinate of the center of the Mohr's circle of radius k. From the Mohr's circle it can be seen that the following relations are true and that they satisfy the yield equations.

$$\sigma x = -p - k \sin 2\phi \tag{7}$$

$$\sigma y = -p + k \sin 2\phi \tag{8}$$

$$\tau xy = k \cos 2\phi \tag{9}$$

Substitution of equations (7-9) into (2) and (3) yields a pair of hyperbolic equations which can be solved for p and ϕ by the method of characteristics. These equations are given below.

$$\frac{\partial p}{\partial x} - 2k \cos(2\phi)\frac{\partial \phi}{\partial x} - 2k \sin(2\phi)\frac{\partial \phi}{\partial y} = 0 \tag{10}$$

$$\frac{\partial p}{\partial y} - 2k \sin(2\phi)\frac{\partial \phi}{\partial x} - 2k \cos(2\phi)\frac{\partial \phi}{\partial y} = 0 \tag{11}$$

The characteristic directions for equations (10) and (11) obtained by the method of characteristics are given by equations (12) and (13).

$$\frac{dy}{dx} = \tan \phi \tag{12}$$

$$\frac{dy}{dx} = \tan \left(\phi + \pi/2\right) \tag{13}$$

The curves defined by these equations represent the directions of maximum shear stress in the material and are called the slip-lines. The two families of curves form an orthogonal net in the material which makes up the slip-line field. The curves of the family denoted by the parameter ϕ will be called α-lines, and those denoted by the parameter $(\phi + \pi/2)$ will be called β-lines. At any point in the (x,y) plane of the material the direction of the algebraically greatest principal stress bisects the right angle between the α and β directions in the first and third quadrants of a right handed (α,β) coordinate system.

The Hencky equations which are another form of the plane-strain equilibrium equations for a material in the plastic state are given below.

$$p + 2k\phi = \text{constant on an } \alpha\text{-line} \tag{14}$$

$$p - 2k\phi = \text{constant on a } \beta\text{-line} \tag{15}$$

The Hencky equations can be used to find the hydrostatic stress anywhere along a slip-line, provided p is known at some point, and the angle ϕ is known along the slip-line.

The characteristics of the velocity equations coincide exactly with the characteristics of the stress equations. Hence, the Geiringer equations for velocity given below are applicable along the slip-lines just as the Hencky equations are.

$$du - v\ d\phi = 0 \quad \text{on an } \alpha\text{-line} \tag{16}$$

$$dv + u\ d\phi = 0 \quad \text{on a } \beta\text{-line} \tag{17}$$

Using the Geiringer equations it is possible to numerically calculate velocities from a slip-line field. However it is often more practical to obtain velocities graphically by constructing a hodograph. A hodograph is a diagram which graphically shows the velocity of every point in the material. For complex slip-line fields the hodograph is usually constructed numerically but for approximate slip-line fields, consisting only of straight lines and circular arcs, the hodograph can be constructed graphically. The hodographs used for the metal cutting problem will be simple enough to construct graphically so it will not be necessary to use numerical techniques.

A simplified slip-line field, constructed of straight lines and circular arcs, is an approximation to a true slip-line field which would probably consist of curved slip-lines. In an actual problem the material flows continuously and a hodograph corresponding to a true slip-line field would also consist of curved lines. However, when a simplified slip-line field is used, the corresponding hodograph will contain velocity discontinuities. Velocity discontinuities may occur when the material crosses a slip-line. At a velocity discontinuity only the component of velocity tangent to the slip-line changes. The normal component of velocity must remain constant across a slip-line.

Another type of discontinuity, often necessary in a simplified slip-line solution, is a stress discontinuity. A stress discontinuity is sometimes required to make the stress in different regions of the material

match up. In reality the stress may be changing through a small region and could be represented by a field of curved slip-lines in that region. However for a simplified solution it is assumed that the change in stress occurs at a line of discontinuity.

The stress conditions at a stress discontinuity can be easily visualized from the stress plane and corresponding Mohr's circle of Figure 3. To satisfy equilibrium the normal stress (σ_n) and the shear stress (τ) must be the same on both sides of the discontinuity. The tangential component of stress changes across the line of discontinuity as does the hydrostatic stress. The magnitude of the change in hydrostatic stress across a stress discontinuity is given by equation (18).

$$\Delta p = 2k \sin 2\Theta \tag{18}$$

A line of stress discontinuity can be oriented in any direction in the material except parallel to a slip-line. If a discontinuity was oriented parallel to a slip-line, the two Mohr's circles of Figure 3 would coincide.

When solving a problem using slip-line theory it is necessary to consider the boundary conditions. One type of boundary condition encountered in metal cutting problems is a stress free surface. On a stress free surface the shear and normal stresses are zero and therefore the tangential stress component must be -2k if the material is in the plastic state. The slip-lines meet a stress free surface at 45°, since there is no shear stress on the surface.

Another type of boundary condition encountered in metal cutting occurs at the tool-workpiece interface. On this surface there can be both shear and normal stresses acting. The shear stress arises from the friction between the tool and the workpiece. If the magnitude of the shear stress is known, the angle at which each family of slip-lines intersects the boundary can be found from the Mohr's circle. In the frictionless case the shear

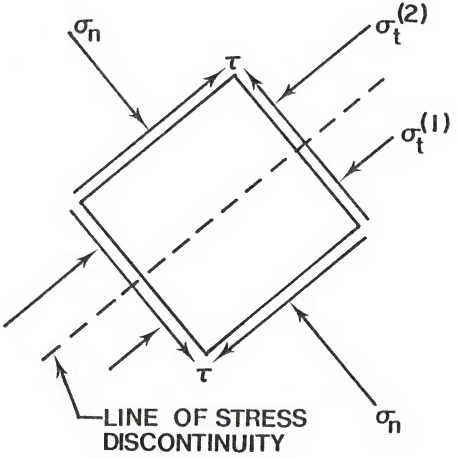

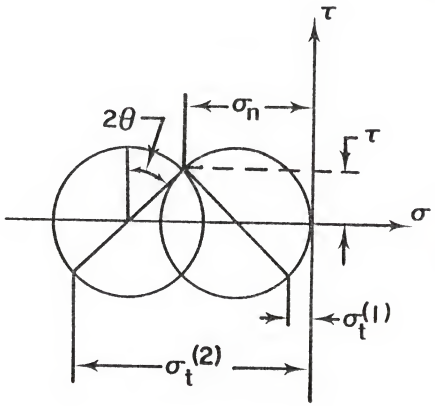

Figure 3

Stress Components at a
Stress Discontinuity

stress is zero and the slip-lines intersect the boundary at 45°. For the other extreme, called sticking friction, the shear stress is equal to k and one family of slip-lines is perpendicular to the boundary while the other family is parallel to it.

The magnitude of the frictional shear stress at the tool-workpiece interface is not known a priori for the metal cutting problem. It is generally agreed that the magnitude of the shear stress depends on the normal stress. Recent theoretical work [22] has been done to determine the relationship between shear and normal stress in the range of normal stresses encountered in metal cutting. Results of this theoretical work will be used when trying to determine the shear stress at the tool-workpiece interface.

In any two-dimensional plasticity problem it may be possible to find many different slip-line fields with stress fields which satisfy the boundary conditions and with valid hodographs. Any of these slip-line fields are upper bound solutions to the problem. To be complete solution, however, there are two more requirements which must be satisfied. The first requirement is that the rate of plastic work done in the deforming material must be positive everywhere. Since the deformation in a slip-line field takes place along the slip-lines, which are in the directions of maximum shear stress, a velocity discontinuity across a slip-line must be in the same direction as the shear stress across the slip-line to ensure that the work done by the shear stress is positive. In a simplified slip-line field all deformation occurs at velocity discontinuities, so it is only necessary to check for positive work at the velocity discontinuities. The second requirement for a complete solution is that the material adjacent to the plastic region is not overstressed. To check this requirement it is necessary to find a stress field in the adjacent regions which satisfies equilibrium without violating

the yield criterion. If this can be done, and the first requirement is also satisfied, then the slip-line field is the complete solution.

SLIP-LINE SOLUTION

The first step in obtaining a slip-line solution was to assume a trial slip-line field. Based on intuition and experimental results, there were certain features which were desired. When the tool is cutting, the slip-line field has to contain a chip. Furthermore, most experiments have indicated a stagnation point on the tool [9], [11]. It was therefore necessary that the slip-line field include a stagnation point above which the material flows upwards along the tool and below which the material flows down the tool. Experiments have also indicated a build up of material ahead of the tool which is called a prow [10]. These features are included in the possible slip-line field of Figure 4.

This slip-line field has a valid hodograph and appeared to be a good solution. However, in determining the shear stresses on the tool face, τ_1 and τ_2, corresponding to the normal stresses σ_1 and σ_2 it was necessary to vary the friction angles η_1 and η_2 independently. From the geometry of the assumed slip-line field it is seen that η_1 and η_2 have a definite geometrical relationship and hence are not independent. Thus, another requirement of the slip-line field is that the friction angles must be independent.

Another trial slip-line field with independent friction angles was developed as shown in Figure 5. With this slip-line field it was possible to calculate upper bounds for the cutting forces F_n and F_t. However, when the upper bounds were minimized the length R approached zero and the stagnation point B moved to the bottom of the tool (point C). The length of the slip-line DB remained constant, and the slip-line field

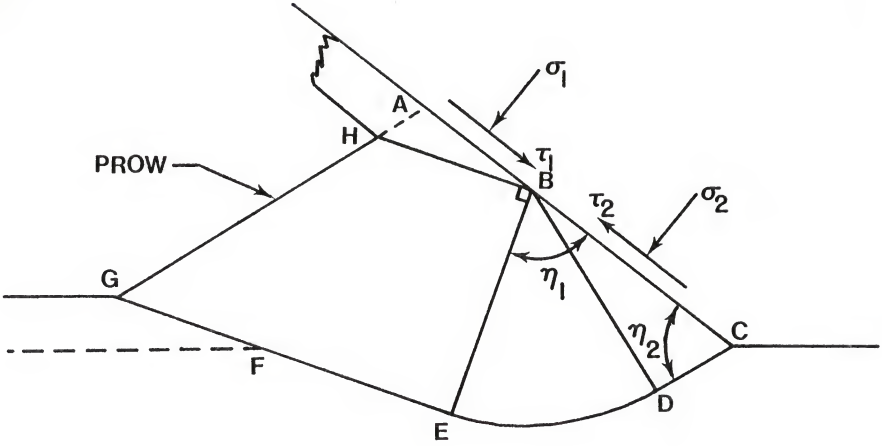

Figure 4

Trial Slip-line Field

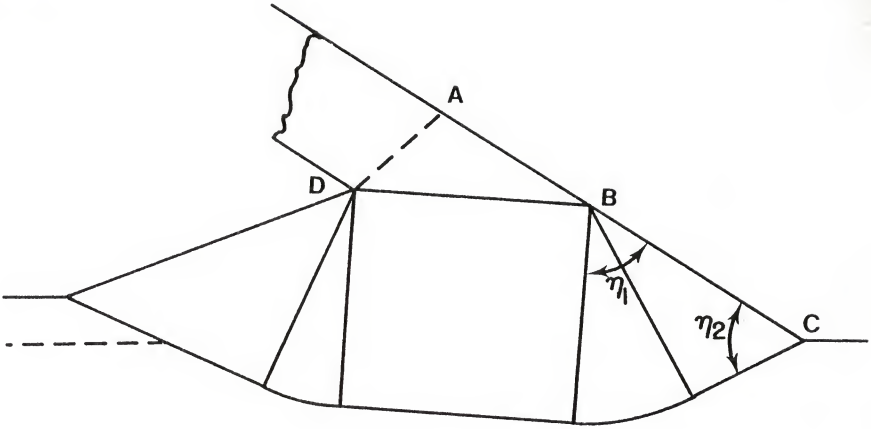

Figure 5

Trial Slip-line Field

was reduced to the single shear plane type (Figure 6) which is used in conventional metal cutting theory. This type of slip-line field is valid for positive rake angles and small negative rake angles. But, for given friction conditions, the shear plane angle ζ decreases as the rake angle becomes more negative. When the rake angle is sufficiently negative, ζ is equal to zero, and the solution is no longer valid. Thus, to obtain a solution which was valid for large negative rake angles and which included a stagnation point, it was necessary to develop a new slip-line field which could not be reduced to the single shear plane type. Numerous slip-line fields were tried but none could be found which met all of the previously discussed requirements and also satisfied equilibrium. The main difficulty was in getting the hydrostatic pressure in adjacent regions to match at the common boundary between the regions. The slip-line field of Figure 7 is the best approximate solution that could be developed using simple slip-line theory.

This slip-line field has variable friction angles, η_1 and η_2, and it cannot be reduced to a single shear plane type slip-line field. However, it contains a pressure mis-match in the region BGH due to the stress discontinuity FG. The pressure along slip-line BE is P_2, but the pressure along slip-lines BH and GH is P_1. It is believed that with a more complex slip-line field the pressures in this region could be matched up to satisfy equilibrium. Thus the pressures P_1 and P_2 are reasonably correct and the stresses on the tool are not appreciably affected by the mis-match of pressures in the region BGH. Although this solution is an approximation, it is believed to be the first slip-line solution which is valid for large negative rake angles and includes a stagnation point.

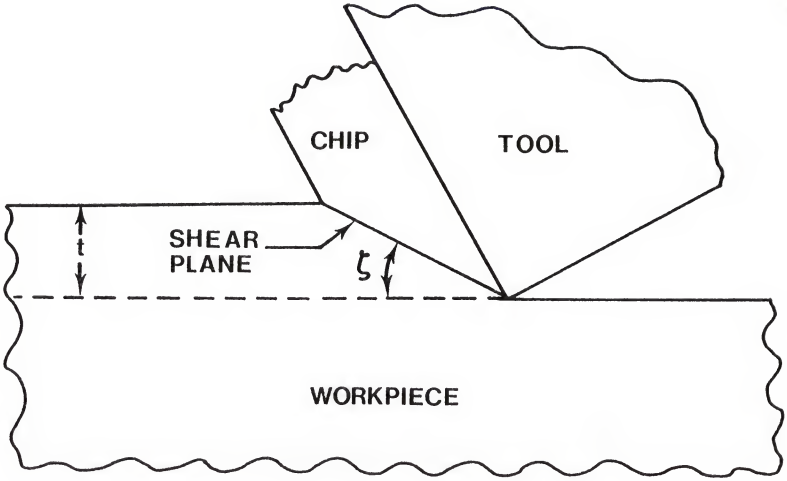

Figure 6

Single Shear Plane Solution

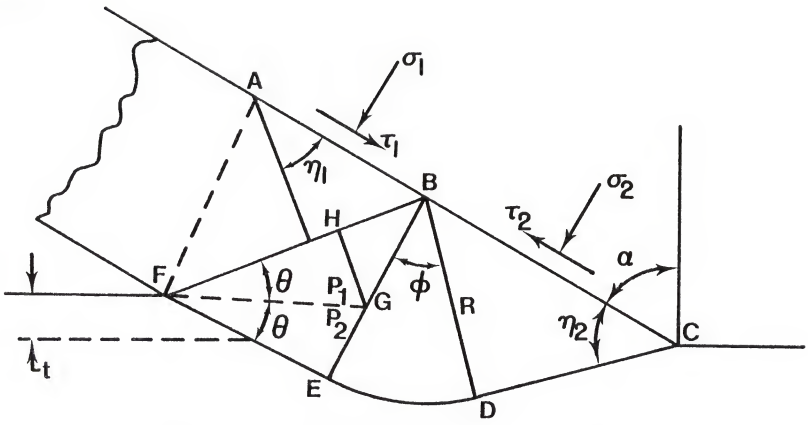

Figure 7

Slip-line Field Solution with
Stress Discontinuity

The slip-line field and the corresponding hodograph are shown in Figure 8. The U vectors in the hodograph represent the velocities of the regions in the slip-line field which have constant velocity. The U* vectors represent the velocity discontinuities which occur along the slip-lines. The arc aa in the hodograph represents the continuous change in velocity from U_1 to U_3 which occurs in the fan DBE. The fan angle ϕ in the slip-line field is equal to the angle of arc aa in the hodograph.

There are several geometrical constraints on the angles α, η_1, η_2, and Θ in the slip-line field of Figure 7 which must be satisfied for the slip-line field and hodograph to be valid. From slip-line theory the friction angles η_1 and η_2 must be less than or equal to 45° so that the frictional stresses are in the proper directions. By observing the slip-line field of Figure 7 it is seen that the sum of α and η_2 must be greater than 90°. If the sum was less than 90°, all of the material entering the slip-line field would be removed as a chip and there would not be a stagnation point on the tool. Thus if η_2 is less than or equal to 45°, the range of α is

$$45^\circ < \alpha < 90^\circ \tag{19}$$

The minimum value of η_2 is dependent on α and thus the range of η_2 is given by the expression

$$(90^\circ - \alpha) < \eta_2 \leq 45^\circ \tag{20}$$

When η_1 is decreased, for fixed values of α and η_2, the depth of cut decreases. Hence the lower bound on η_1 is obtained when the depth of cut is reduced to zero. For zero depth of cut, η_1 is given by the following expression which has been verified numerically.

$$\eta_1 = \alpha - \sin^{-1}\left[\frac{\cos(\alpha)}{\sin(\eta_2)}\right] \tag{21}$$

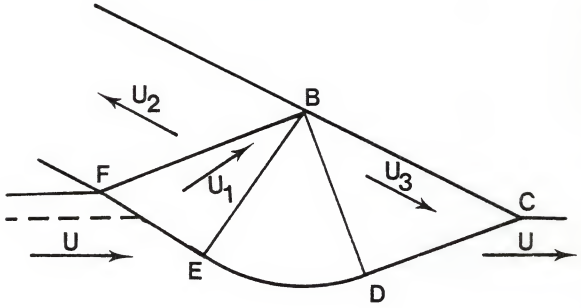

SLIP-LINE FIELD

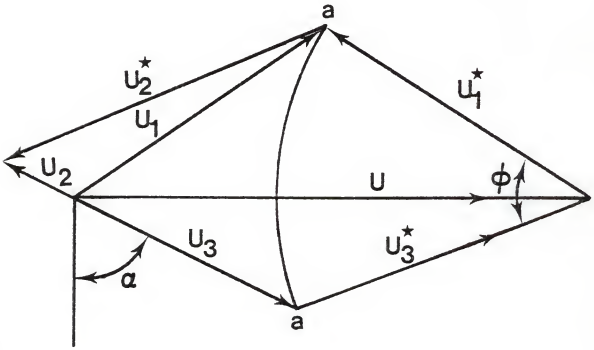

HODOGRAPH

Figure 8

Slip-line Field with Hodograph

Therefore the permissable range of η_1 is

$$\alpha - \sin^{-1}\left[\frac{\cos(\alpha)}{\sin(\eta_1)}\right] < \eta_1 \leq 45^{\circ} \tag{22}$$

The value of θ may approach a maximum of 45°. The minimum value of θ occurs when the velocity U_1 (Figure 8) becomes parallel to the slip-line BF. On the hodograph this means that U_1 and U_2* coincide. In this case the material with velocity U_1 will not cross the slip-line and hence no chip will be formed. An expression for the minimum value of θ can be obtained from the hodograph of Figure 9.

Using the law of sines,

$$\frac{U}{\sin(\pi - \eta_2)} = \frac{U_3^*}{\sin(\pi/2 - \alpha)} \tag{23a}$$

or

$$U_3^* = \frac{U\cos(\alpha)}{\sin(\eta_2)} \tag{23b}$$

and

$$\frac{U}{\sin(\pi - 2\theta\,\text{min})} = \frac{U_1^*}{\sin(\alpha - \eta_1)} \tag{23c}$$

or

$$U_1^* = \frac{U\sin(\alpha - \eta_1)}{\sin(2\theta\,\text{min})} \tag{23d}$$

But since U_1* and U_3* occur on the same slip-line their magnitudes must be equal. Combining equations (23b) and (23d) and solving for θmin leads to

$$\theta\text{min} = \tfrac{1}{2}\sin^{-1}\left[\frac{\sin(\alpha - \eta_1)\sin(\eta_2)}{\cos(\alpha)}\right] \tag{24}$$

Thus the range of θ is

$$\tfrac{1}{2}\sin^{-1}\left[\frac{\sin(\alpha - \eta_1)\sin(\eta_2)}{\cos(\alpha)}\right] < \theta < 45^{\circ} \tag{25}$$

One of the requirements of a complete slip-line solution is that the rate of plastic work done everywhere in the material must be positive. In the slip-line field of Figure 7 all of the plastic work takes place at the slip-lines where the velocity discontinuities occur. Thus the check for positive work is done by checking the direction of the shear stresses at the velocity discontinuities. For positive work to occur, the direction

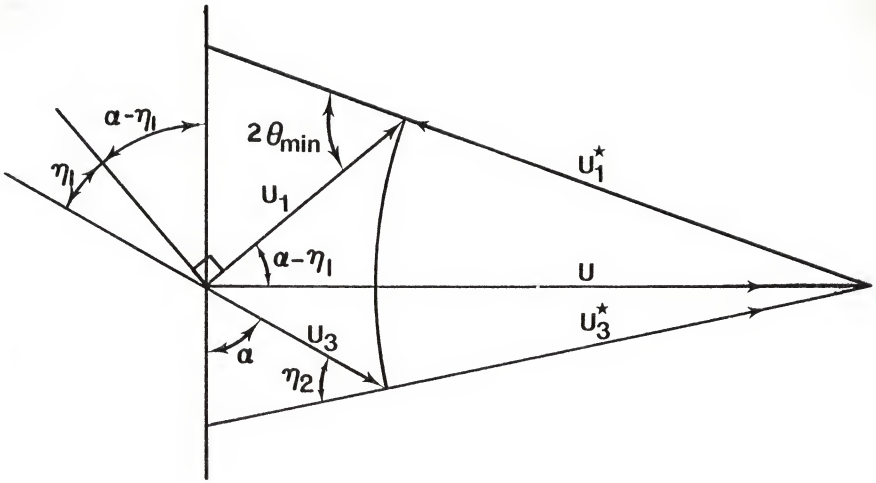

Figure 9

Hodograph for Determining θ_{min}

of the shear stress across a velocity discontinuity must be the same as the direction of the velocity discontinuity. Figure 10 shows the directions of the shear stresses on elements at the various slip-lines where discontinuities occur. From Figure 10 and the hodograph of Figure 8 it is observed that all of the shear stresses across velocity discontinuities are in the same direction as the discontinuities and therefore all of the plastic work done is positive.

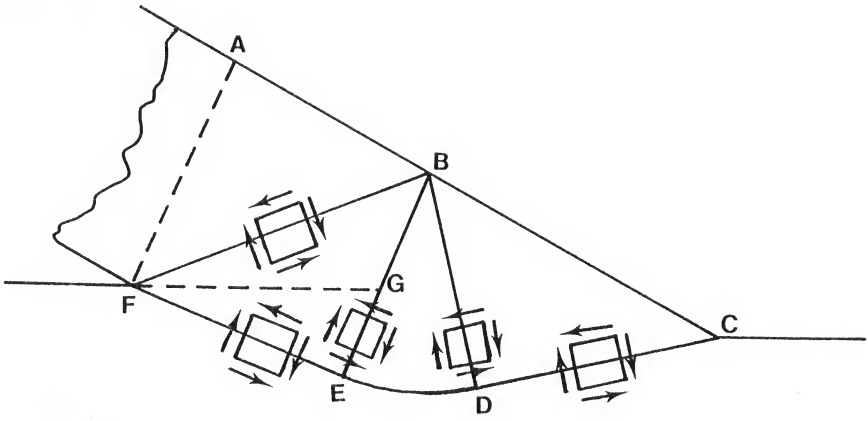

Figure 10

Directions of Shear Stresses

CUTTING FORCE COMPONENTS

The cutting forces were found using the slip-line field of Figure 7. The first step in calculating the cutting forces was to compute the stresses acting on the work material. The stresses σ_1, σ_2, τ_1, and τ_2 are shown in Figure 7 in the directions in which they act on the material. These directions coincide with the directions of the external forces which must be applied to the tool to make the cut. Hence calculating the forces due to σ_1, σ_2, τ_1, and τ_2 will yield the desired cutting forces in the proper directions.

The stresses σ_1 and τ_1 can be found in terms of the friction angle η_1 using the Mohr's circle of Figure 11. The chip material which is to the left of the stress discontinuity AF in Figure 7 is stress free and thus has a Mohr's circle which is a point located at the origin of the σ-τ coordinate system. The material on the other side of the stress discontinuity is in the plastic state and has the Mohr's circle of Figure 11. The state of stress at the stress discontinuity is shown in Figure 12a. By rotating through the proper angle $(90^{\circ} + 2\eta_1)$ on the Mohr's circle, the stress components acting on the material adjacent to the tool are obtained. (Figure 12b) The stresses are given mathematically by the following equations.

$$\sigma_1 = k\,[1 + \sin(2\eta_1)] \tag{26}$$

$$\tau_1 = k \cos(2\eta_1) \tag{27}$$

The other stresses, σ_2 and τ_2, were found from the Mohr's circles of Figure 13 together with the Hencky equations and equation (18) for the change in hydrostatic stress across a stress discontinuity. In Figure 13, point A represents the normal and shearing stresses at slip-line BF of

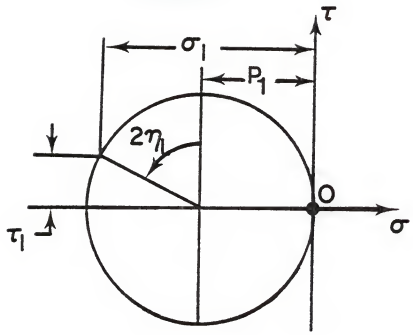

Figure 11

Mohr's Circle for σ_1 and τ_1

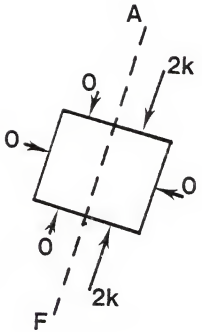

a. Stress Discontinuity AF

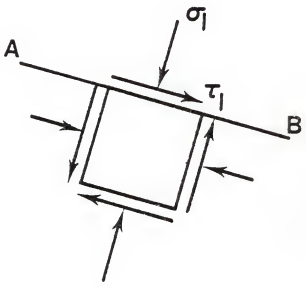

b. Stresses on the Tool at Section AB

Figure 12

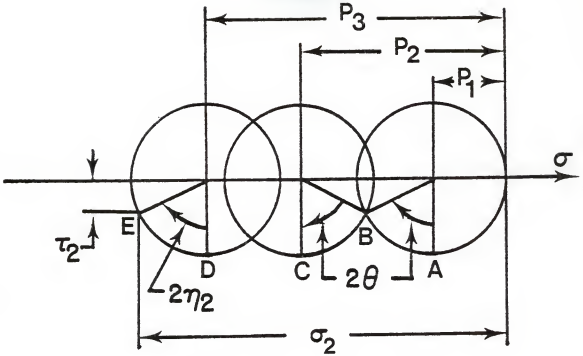

Figure 13

Mohr's Circle for σ_2 and τ_2

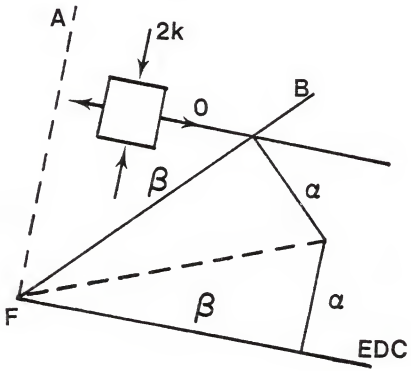

Figure 14

Determination of α and
β Directions

Figure 7. By rotating on the circle through the angle 2θ the stresses at the discontinuity FG are obtained (Point B). Across the stress discontinuity a new Mohr's circle is required. By rotating on the new circle through the angle 2θ the stresses at slip-line EF are obtained (Point C). The change in hydrostatic stress Δp due to the stress discontinuity is obtained from equation (18) as

$$\Delta p = 2k \sin 2\theta \tag{18}$$

The slip-line FEDC is a continuous slip-line and hence the hydrostatic stress can be found anywhere along the slip-line given the stress at some point on the slip-line and the angular change of the slip-line. By examining the stresses in the region ABF of Figure 14 it is found that slip-line FEDC is a β slip-line since the direction of the algebraically greatest principal stress bisects the right handed α-β coordinate system in the first and third quadrants. Hence the Hencky equation for a β characteristic can be used to find the change in hydrostatic stress from segment EF to segment CD. The Hencky euqation is of the form

$$p - 2k\phi = \text{constant} \tag{15}$$

Thus

$$P_2 - 2k\phi_2 = C \tag{28}$$

and

$$P_3 - 2k\phi_3 = C \tag{29}$$

Combining (28) and (29) gives

$$P_3 - P_2 = 2k\ (\phi_3 - \phi_2) \tag{30}$$

or

$$P_3 - P_2 = 2k\phi \tag{31}$$

The final step in determining the stress components σ_2 and τ_2 is to rotate from point D to point E on the Mohr's circle of Figure 13. Thus the stress components can be written as

$$\sigma_2 = k\ [1 + 2\phi + 2 \sin (2\theta) + \sin (2\eta_2)] \tag{32}$$

$$\tau_2 = k \cos (2\eta_2) \tag{33}$$

To compute the cutting forces from the stresses on the tool face it is necessary to know the area on which the stresses act. Assuming the tool is of unit width, the area is equal to the length of the tool. The length of the tool can be divided into two parts, ℓ_1 and ℓ_2. The length over which σ_1 and τ_1 act is ℓ_1, and the length over which σ_2 and τ_2 act is ℓ_2. (Figure 15) These lengths can be determined in terms of the radius (R) of the fan in the slip-line field.

$$\ell_1 = \frac{R}{\sqrt{2} \sin (2\theta) \sin (\eta_1 + \pi/4)} \tag{34}$$

$$\ell_2 = \frac{R}{\sin (\eta_2)} \tag{35}$$

The cutting force components which are of interest are the force tangential to the cutting direction and the force normal to the cutting direction. These components will be labeled F_t and F_n respectively. (Figure 15) The expressions for the force components are given below.

$$F_t = (\sigma_1 \ell_1 + \sigma_2 \ell_2) \cos(\alpha) + (\tau_2 \ell_2 - \tau_1 \ell_1) \sin(\alpha) \tag{36}$$

$$F_n = (\sigma_1 \ell_1 + \sigma_2 \ell_2) \sin(\alpha) + (\tau_1 \ell_1 - \tau_2 \ell_2) \cos(\alpha) \tag{37}$$

The dimensions of these forces are force/length since the tool area was calculated per unit width of tool. For convenience the dimensionless forms $\frac{F_{t,n}}{tk}$ of the force components will be used. The depth of cut, t, can be derived from the geometry of the slip-line field as

$$t = R \left[\frac{\cos (\alpha)}{\sin (\eta_2)} - \frac{\sin (\alpha - \eta_1)}{\sin (2\theta)} \right] \tag{38}$$

By substituting for the stresses and lengths in equations (36) and (37) and using equation (38) for t the dimensionless forces are given as follows.

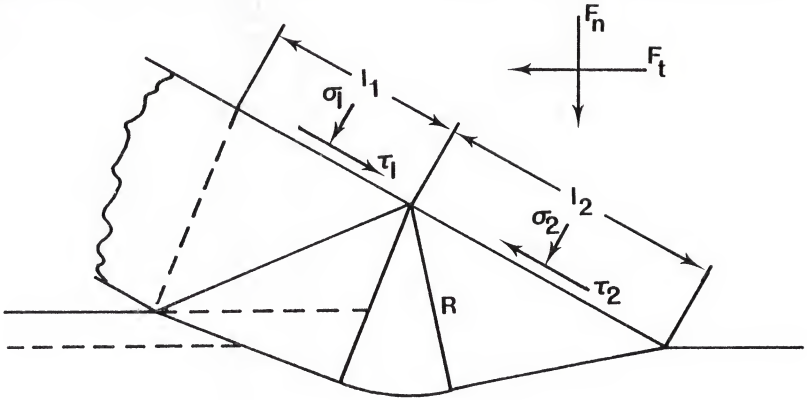

Figure 15

Determination of Cutting Forces

$$\frac{F_t}{tk} = \left[\left[\frac{1 + \sin(2\eta_1)}{\sqrt{2}\sin(2\theta)\sin(\eta_1 + \pi/4)} + \frac{1 + 2\phi + 2\sin(2\theta) + \sin(2\eta_2)}{\sin(\eta_2)}\right]\left[\cos(\alpha)\right] + \left[\frac{\cos(2\eta_2)}{\sin(\eta_2)} - \frac{\cos(2\eta_1)}{\sqrt{2}\sin(2\theta)\sin(\eta_1 + \pi/4)}\right]\left[\sin(\alpha)\right]\right] \Big/ \left[\frac{\cos(\alpha)}{\sin(\eta_2)} - \frac{\sin(\alpha - \eta_1)}{\sin(2\theta)}\right] \quad (39)$$

$$\frac{F_n}{tk} = \left[\left[\frac{1 + \sin(2\eta_1)}{\sqrt{2}\sin(2\theta)\sin(\eta_1 + \pi/4)} + \frac{1 + 2\phi + 2\sin(2\theta) + \sin(2\eta_2)}{\sin(\eta_2)}\right]\left[\sin(\alpha)\right] + \left[\frac{\cos(2\eta_1)}{\sqrt{2}\sin(2\theta)\sin(\eta_1 + \pi/4)} - \frac{\cos(2\eta_2)}{\sin(\eta_2)}\right]\left[\cos(\alpha)\right]\right] \Big/ \left[\frac{\cos(\alpha)}{\sin(\eta_2)} - \frac{\sin(\alpha - \eta_1)}{\sin(2\theta)}\right] \quad (40)$$

The fan angle ϕ can be derived in terms of the friction angles and θ as

$$\phi = 2\theta + \eta_1 + \eta_2 - \pi/2 \quad (41)$$

Thus the dimensionless forces are dependent only on the back rake angle α, the friction angles η_1 and η_2, and θ.

Another quantity which is of interest is the mean pressure ratio. The mean pressure ratio for this problem is the average normal pressure (P_m) on the tool divided by the pure shear yield stress (k). The mean pressure ratio is given by the following expression.

$$\frac{P_m}{k} = \frac{1}{k}\frac{\sigma_1 \ell_1 + \sigma_2 \ell_2}{\ell_1 + \ell_2} \quad (42)$$

By substituting for the stresses and lengths the mean pressure ratio becomes

$$\frac{P_m}{k} = \frac{\frac{1 + \sin(2\eta_1)}{\sqrt{2}\sin(2\theta)\sin(\eta_1 + \pi/4)} + \frac{1 + 2\phi + 2\sin(2\theta) + \sin(2\eta_2)}{\sin(\eta_2)}}{\frac{1}{\sqrt{2}\sin(2\theta)\sin(\eta_1 + \pi/4)} + \frac{1}{\sin(\eta_2)}} \quad (43)$$

NUMERICAL RESULTS: FRICTIONLESS CASE

The first case to be considered was the frictionless case. In this case the shear stresses τ_1 and τ_2 are zero and the friction angles η_1 and η_2 are 45°. The negative rake angle was varied from a minimum of 45° to a maximum value at which the depth of cut, t, in the slip-line field became zero. The following equation which is a form of equation (21) is a relationship between the rake angle and the friction angles when the depth of cut is zero.

$$\sin(\eta_1 - \alpha) + \frac{\cos(\alpha)}{\sin(\eta_2)} = 0 \tag{44}$$

Solving equation (44) for α yields

$$\alpha = \tan^{-1}\left[\tan(\eta_1) + \frac{1}{\cos(\eta_1)\sin(\eta_2)}\right] \tag{45}$$

With the friction angles equal to 45° equation (45) gives a value of approximately 71.6° for the maximum allowable negative rake angle in the frictionless case.

Equations (39) and (40) for the dimensionless forces F_t and F_n are only dependent on the rake angle and θ for the frictionless case since η_1 and η_2 are fixed. Hence for a given rake angle the only variable is θ. In carrying out the numerical results it was found that for any rake angle the dimensionless forces had definite minimums with respect to θ. The relationship between F_t and θ for a negative rake angle of 60° shown in Figure 16 is typical of the variation of both F_t and F_n for any rake angle. Since F_t and F_n are upper bounds of the actual cutting forces, the minimum values of the forces with respect to θ were calculated for various rake angles. The results are plotted in Figure 17.

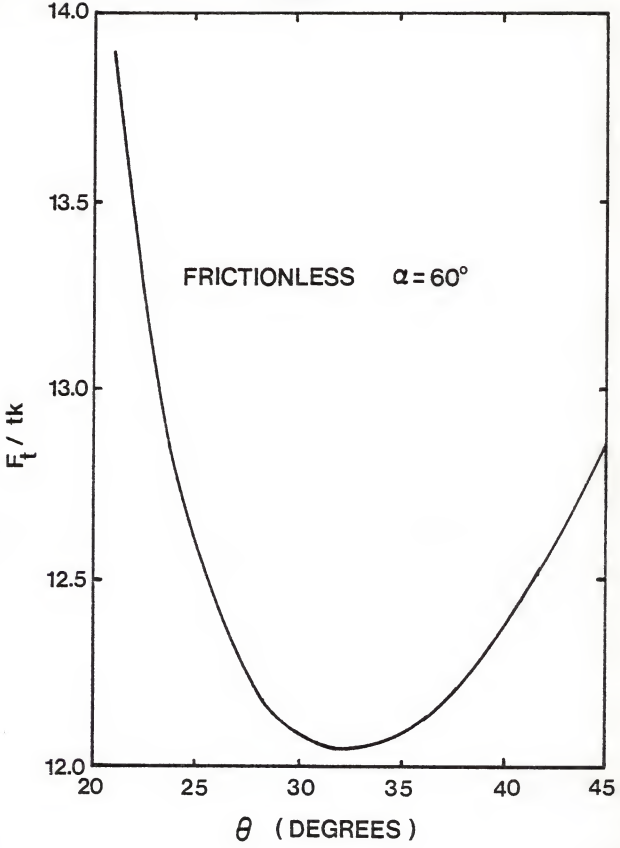

Figure 16

Variation of Tangential Cutting Force with respect to θ

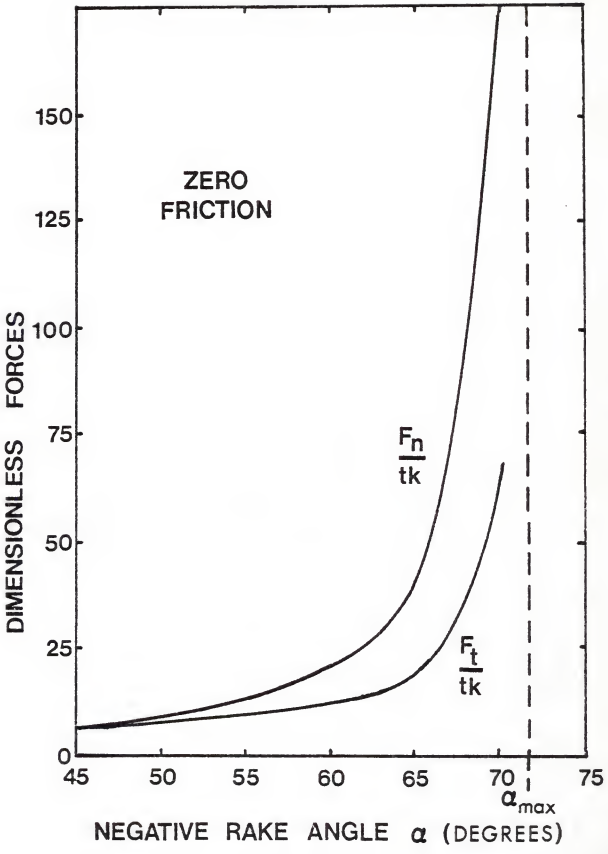

Figure 17

Minimum Dimensionless Cutting Forces

Varying θ with α, η_1, and η_2 fixed actually varies the depth of cut. Thus, minimizing with respect to θ determines the depth of cut which requires the smallest cutting force per unit depth of cut. The dimensionless parameter t/R was calculated form equation (38). Figure 18 shows how the depth of cut which requires the least cutting force for a given rake angle varies with respect to the rake angle.

As expected, the required cutting forces increase as the rake angle becomes more negative, and the normal force which is required to force the tool down into the workpiece increases much faster than the tangential force. As the rake angle approaches its maximum value the depth of cut goes to zero and thus the dimensionless forces become infinite.

The mean pressure ratio which was also minimized with respect to θ is plotted in Figure 19. In Bowden and Tabor [23] a mean pressure ratio defined as P_m/Y, where Y is the yield stress in pure tension, is given for indentation of a hard spherical ball into work-hardened steel. Their experimentally oriented ratio is 2.8 which corresponds to P_m/k of approximately 4.9 as shown in Figure 19. The fact that the experimentally obtained mean pressure ratio for indentation is in the range of mean pressure ratios obtained for frictionless negative rake cutting is encouraging since the two processes are similar.

A slip-line field and hodograph for frictionless cutting with a negative rake angle of 60° is shown in Figure 20. In this case θ is equal to 32.0° and t/R is equal to 0.42.

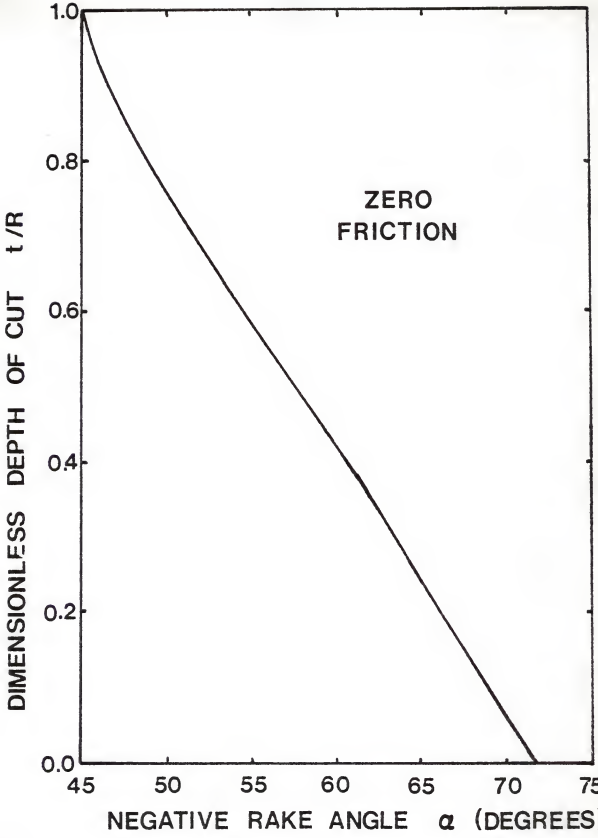

Figure 18

Depth of Cut versus
Negative Rake Angle

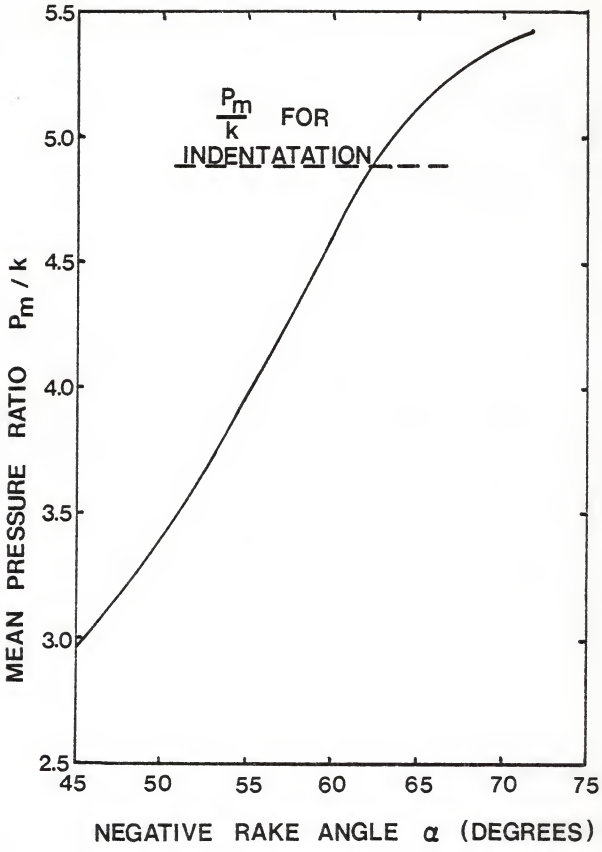

Figure 19

Mean Pressure Ratio versus
Negative Rake Angle

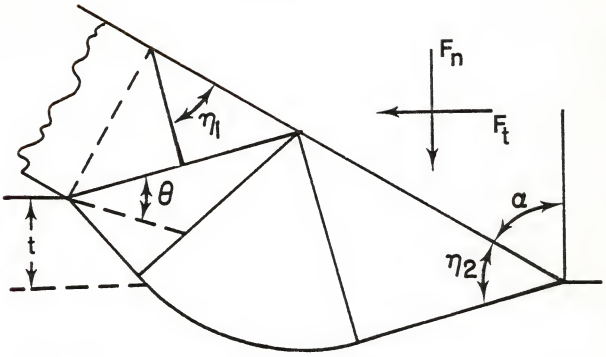

SLIP-LINE FIELD

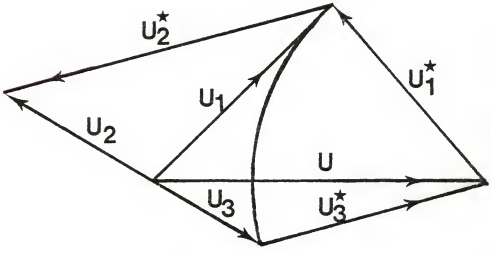

HODOGRAPH

Figure 20

Frictionless Cutting with
α Equal to 60^o

FRICTION AT HIGH NORMAL PRESSURES

Friction between the tool and the workpiece is a very significant factor in determining the forces involved in metal cutting. In ordinary cutting theory the frictional shear stress on the cutting tool is usually assumed to be proportional to the normal stress. This is Amonton's law of friction which is only applicable at low normal stress. In negative rake metal cutting, the normal stresses are very high and thus a relationship between friction and normal stress at high normal pressures is necessary.

It is a generally accepted fact that the shear stress within the work material cannot exceed the yield stress. Thus, for a material with constant yield stress, the relation between frictional shear stress and normal stress must appear as illustrated in Figure 21. The relationship is linear for low values of normal stress, but for higher normal stress, the shear stress reaches a limiting value.

An exact relation for the shape of this curve has not been found but a slip-line solution has been carried out by Wanheim, et al [22] which appears to be a good approximation. The results are given in graphical form, but for purposes of analysis it is more convenient to have equations which adequately approximate the results.

Figure 7 of Wanheim shows graphically the real area of contact A_R as a function of dimensionless normal stress $(\frac{\sigma n}{2k})$ for various values of the adhesion coefficient m. The limit of proportionality is given by

$$\left(\frac{\sigma n}{2k}\right)_{lim} = \frac{\sqrt{2}\ [1 + \pi/2 + 2\xi + \sin 2\xi]}{2\sqrt{2} + 4 \sin \xi} \tag{46}$$

where

$$m = \cos 2\xi \tag{47}$$

and

$$m \neq 0$$

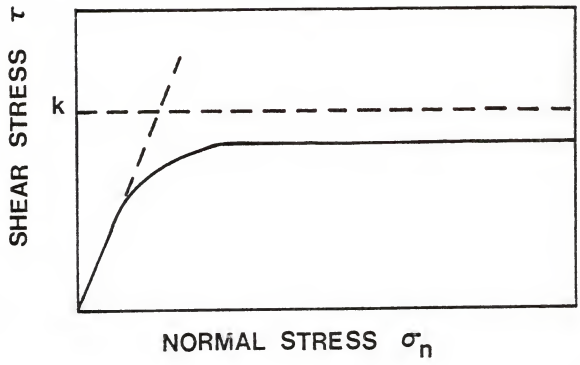

Figure 21

Relation between Frictional Shear Stress and Normal Stress

m	$A_{R_{lim}}$	ξ (Radians)	$(\frac{\sigma_n}{2k})_{lim}$	Slope
0.34	0.55	0.61194	1.3063	0.421
0.50	0.58	0.52360	1.3133	0.442
0.64	0.63	0.43815	1.3173	0.474
0.77	0.67	0.34598	1.3182	0.508
0.87	0.73	0.25780	1.3154	0.555
0.94	0.80	0.17408	1.3094	0.611
1.00	1.00	0.00000	1.2854	0.778

Table I

Numerical Values from Figure 7 [22]

The values of A_R at the limit of proportionality as read from Figure 7 of Wanheim are given in Table I. The following equation represents these values reasonably well as shown in Figure 22.

$$A_{R_{lim}} \simeq 1 - 0.52\ (1 - m)^{0.325} \tag{48}$$

The nominal dimensionless friction is given by

$$\frac{\tau}{k} = m\ A_R \tag{49}$$

Thus, in the linear range the relation between frictional stress and normal stress is given by

$$\frac{\tau}{k} = \mu\ \frac{\sigma n}{2k} \tag{50}$$

where

$$\mu = \frac{m\ A_{R_{lim}}}{\left(\frac{\sigma n}{2k}\right)_{lim}} \tag{51}$$

for

$$0 \leq \frac{\sigma n}{2k} \leq \left(\frac{\sigma n}{2k}\right)_{lim}$$

The real area of contact approaches 1 as $\left(\frac{\sigma n}{2k}\right)$ approaches infinity. Therefore an exponential form will be assumed for A_R beyond $\left(\frac{\sigma n}{2k}\right)_{lim}$.

$$A_R = 1 - \beta_1\ e^{-\beta_2\ \left(\frac{\sigma n}{2k}\right)} \tag{52}$$

for

$$\left(\frac{\sigma n}{2k}\right)_{lim} \leq \frac{\sigma n}{2k}$$

To find the two constants, β_1 and β_2, two equations are required. The first equation is obtained by evaluating equation (52) at $\left(\frac{\sigma n}{2k}\right)_{lim}$.

$$A_{R_{lim}} = 1 - \beta_1\ e^{-\beta_2\ \left(\frac{\sigma n}{2k}\right)_{lim}} \tag{53}$$

The second equation is obtained from the slope of the A_R curve at the proportional limit.

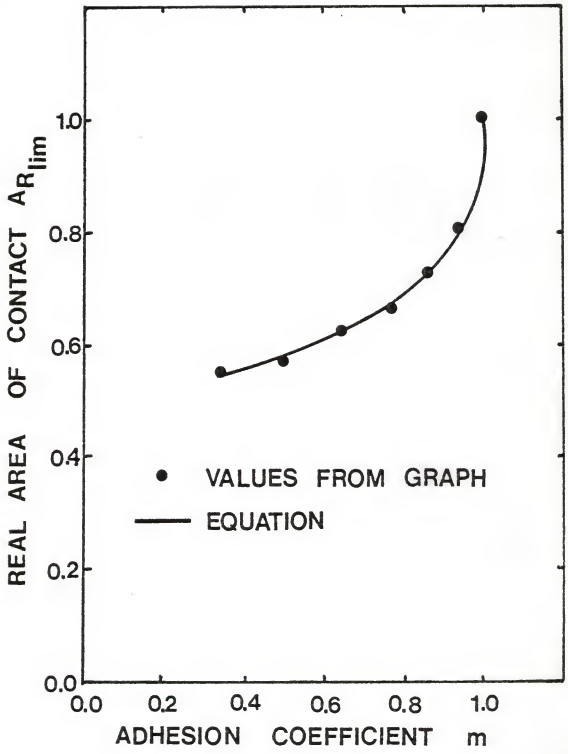

Figure 22

Analytical Representation of the Real Area of Contact at the Proportional Limit versus Adhesion Coefficient

$$\left.\frac{dA_R}{d(\frac{\sigma n}{2k})}\right|_{(\frac{\sigma n}{2k})_{lim}} = \frac{A_{R_{lim}}}{(\frac{\sigma n}{2k})_{lim}} \tag{54}$$

Differentiating equation (52) with respect to $(\frac{\sigma n}{2k})$ and evaluating at $(\frac{\sigma n}{2k})_{lim}$ yields

$$\beta_1 \beta_2 e^{-\beta_2 (\frac{\sigma n}{2k})_{lim}} = \frac{A_{R_{lim}}}{(\frac{\sigma n}{2k})_{lim}} \tag{55}$$

By solving equation (55) for β_1 and substituting into (53), β_2 is obtained as

$$\beta_2 = \frac{A_{R_{lim}}}{(1 - A_{R_{lim}})\ (\frac{\sigma n}{2k})_{lim}} \tag{56}$$

Then from equation (53) β_1 is given by

$$\beta_1 = (1 - A_{R_{lim}})\ e^{\beta 2\ (\frac{\sigma n}{2k})_{lim}} \tag{57}$$

The above equations give a theoretical relationship between the frictional shear stress and the normal stress for a material with constant yield stress k in terms of the adhesive friction coefficient m.

NUMERICAL RESULTS: CUTTING WITH FRICTION

The numerical results were obtained by applying the theory of friction from the previous section to the approximate slip-line solution. From equation (19) it is seen that σ_1 cannot exceed 2k, and thus $\frac{\sigma_1}{2k}$ will not exceed $(\frac{\sigma n}{2k})_{lim}$, as given by equation (46), for all values of adhesion coefficient m. Hence the frictional shear stress τ_1 is given by equations (50) and (51) as

$$\frac{\tau_1}{k} = m\, A_{R_{lim}} \frac{\frac{\sigma_1}{2k}}{(\frac{\sigma n}{2k})_{lim}} \tag{58}$$

From the slip-line solution, τ_1 is given as

$$\frac{\tau_1}{k} = \cos\ (2\eta_1) \tag{59}$$

Combining equations (58) and (59) and substituting equation (19) for σ_1 yields the following equation for η_1 in terms of m.

$$\cos\ (2\eta_1) = \frac{m\ A_{R_{lim}}}{2\ (\frac{\sigma n}{2k})_{lim}} [1 + \sin\ (2\eta_1)] \tag{60}$$

This equation was solved numerically for η_1 at given values of m, and the shear stress τ_1 was calculated from equation (59).

From equation (25) for the normal stress on the lower section of the tool, it is not obvious whether the magnitude of $\frac{\sigma_2}{2k}$ is less than or greater than $(\frac{\sigma n}{2k})_{lim}$. However it was assumed that $\frac{\sigma_2}{2k}$ was greater than $(\frac{\sigma n}{2k})_{lim}$ and thus equation (52) was used to determine the real area of contact A_R. This assumption was checked and found to be true for every case. Using equation (52), the frictional shear stress τ_2 is obtained as

$$\frac{\tau_2}{k} = m \left[1 - \beta_1 e^{-\beta_2 \left(\frac{\sigma_2}{2k}\right)}\right] \tag{61}$$

From the slip-line solution τ_2 is given by

$$\frac{\tau_2}{k} = \cos (2\eta_2) \tag{62}$$

Combining equations (61) and (62) yields the following equation for η_2 in terms of m and σ_2.

$$\cos (2\eta_2) = m \left[1 - \beta_1 e^{-\beta_2 \left(\frac{\sigma_2}{2k}\right)}\right] \tag{63}$$

The normal stress σ_2 is dependent on η_1, η_2, and θ. In solving for η_2 the value of η_1 obtained from equation (61) is used. The value of θ is dependent on α and η_2 and thus it cannot be obtained directly. A double iteration was required to solve equation (63) for η_2. First, equation (63) was solved by an iterative process using an arbitrarily assumed value of θ equal to 30°. Then, for a given value of α, the dimensionless forces were calculated and minimized with respect to θ. The new value of θ corresponding to the minimum cutting forces was then used to solve equation (63) for a new value of η_2. This process was repeated until the change in θ was less than 0.01° which usually required 3 iterations. The value of η_2 was then used to calculate τ_2 from equation (62). The computer program used for the numerical work is listed in Appendix A.

The maximum allowable negative rake angle, α_{max}, for a given adhesion coefficient was calculated from equation (45). The minimum negative rake angle, α_{min}, is given by

$$\alpha_{min} = (90^\circ - \eta_2) \tag{64}$$

These expressions for the extremes of α both contain the friction angle η_2. Since η_2 is dependent on α, the equations for α_{max} and α_{min} were solved within the iteration used to find η_2. The value of η_2 used to solve equations

(45) and (64) was the value obtained from an α equal to the average of α_{max} and α_{min} from the previous time through the iteration. The results are plotted in Figure 23 for a range of adhesion coefficients from 0.5 to 1.0. It is believed that the adhesion coefficient will be within this range for most cutting conditions.

To observe the effect of varying friction, a negative rake angle of 72° was chosen so that the adhesion coefficient could be varied from 0.5 to 0.8. The variations of the shear stresses, normal stresses, and dimensionless forces with respect to m are shown in Figures 24, 25, and 26 respectively. Numerical values are given in Table II of Appendix B.

The effect of varying the rake angle for a constant adhesion coefficient was found to be similar to the frictionless case. The relation between the dimensionless forces and the negative rake angle for m equal to 0.7 is shown in Figure 27. The slip-line field for m equal to 0.7 and the negative rake angle equal to 71° is shown to scale in Figure 28.

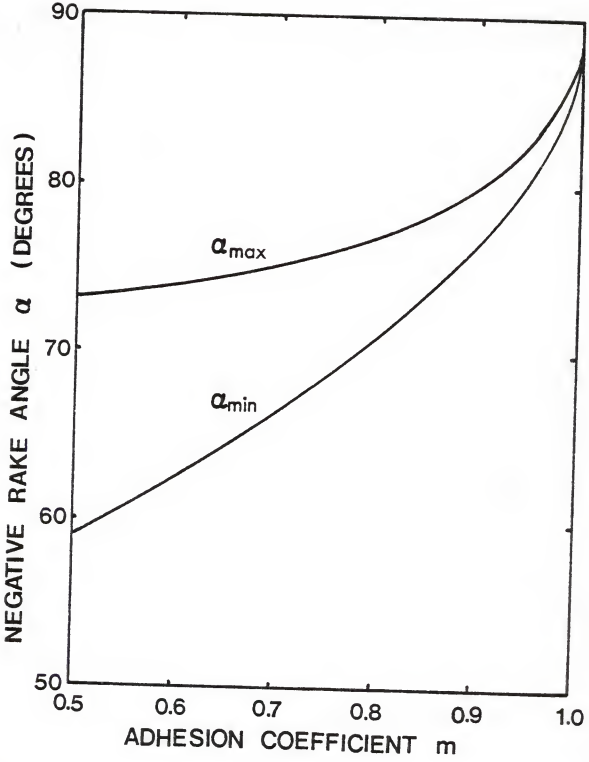

Figure 23

Maximum and Minimum Allowable
Negative Rake Angles

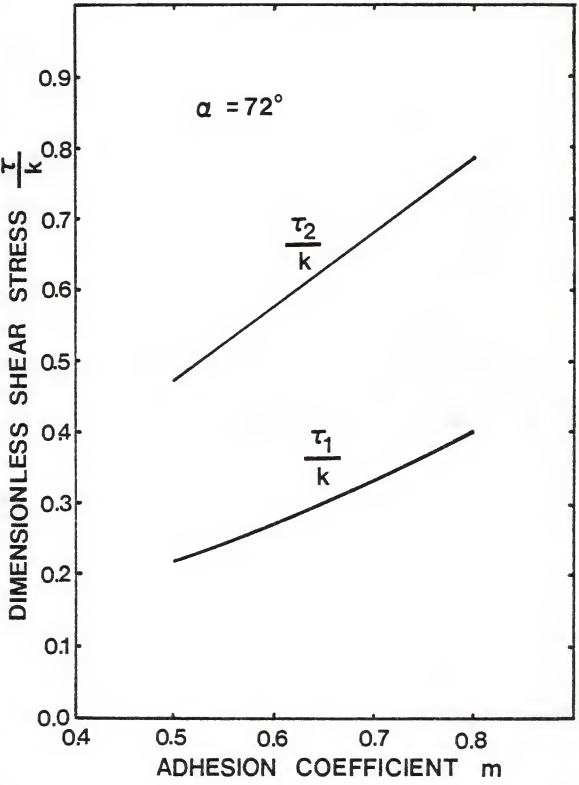

Figure 24

Shear Stresses versus Adhesion Coefficient
with Constant Rake Angle

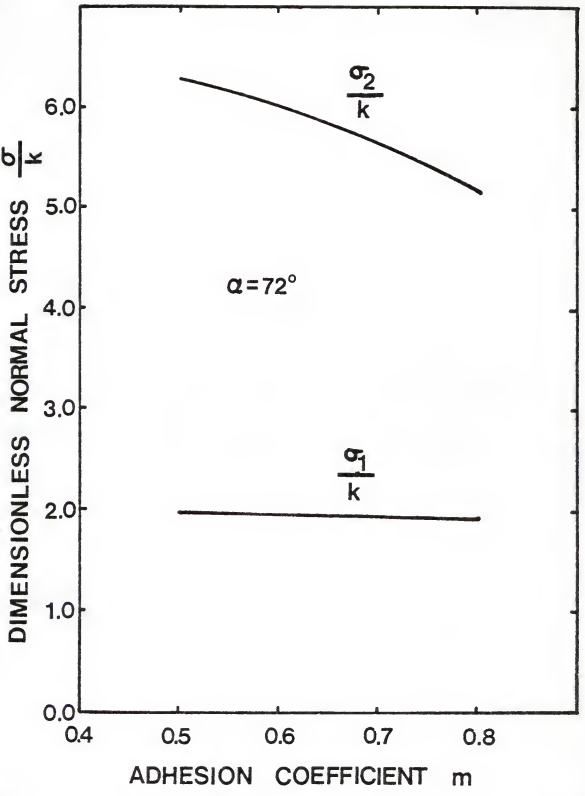

Figure 25

Normal Stresses versus Adhesion Coefficient
with Constant Rake Angle

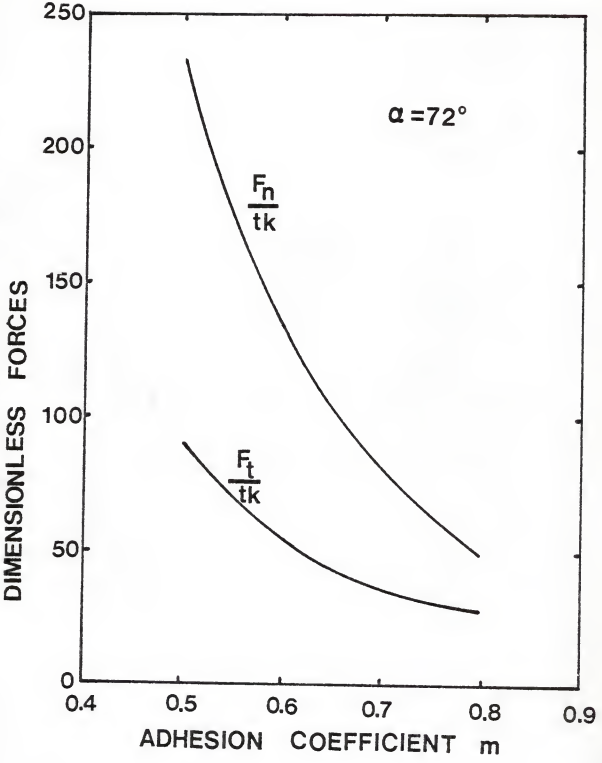

Figure 26

Dimensionless Forces versus Adhesion Coefficient
with Constant Rake Angle

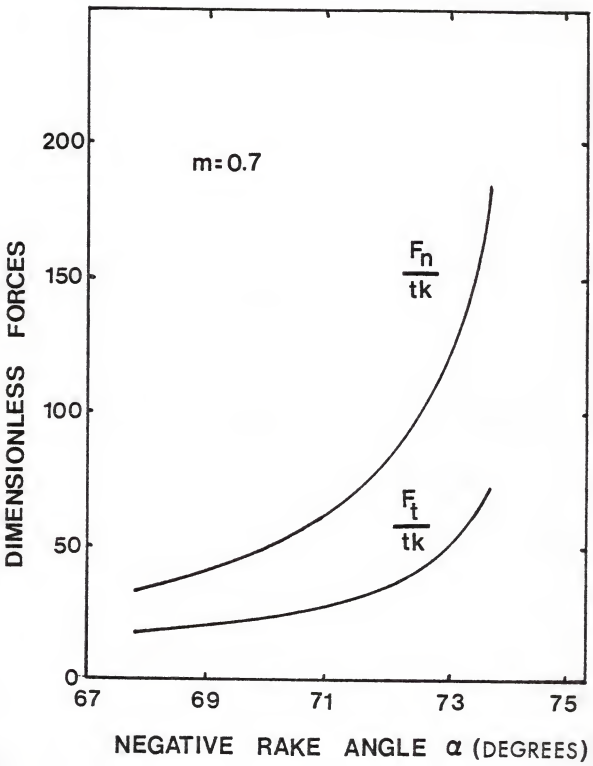

Figure 27

Dimensionless Forces versus Negative Rake Angle
with Constant Adhesion Coefficient

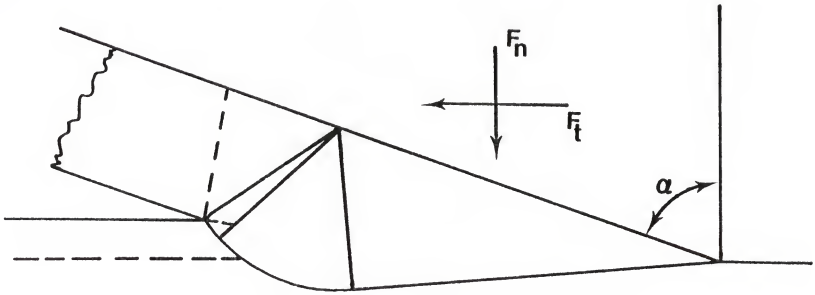

$m = 0.7$

$\alpha = 71°$

$\frac{F_t}{tk} = 27.0 \quad \frac{F_n}{tk} = 58.8$

Figure 28

Slip-line Field

CONCLUSIONS

The slip-line solution which was developed is believed to be a good approximate solution to the large negative rake cutting problem. Furthermore it appears to be the first slip-line solution which applies to large negative rake angles and considers the two way flow of material on the rake face. Although the solution is not exact, it allows for the extension of metal cutting theory to negative rake angles beyond the range covered by conventional metal cutting theory. The belief that the solution is a good approximation is supported by the numerical results.

The numerical results indicate a maximum negative rake angle, depending on the adhesion coefficient, beyond which it is impossible to form a chip. In reality there is probably no well-defined rake angle at which chips cease to form, however some experimenters [8] [11] have reported values of negative rake angle at which chips will not form under certain cutting conditions. They report that beyond the critical rake angle ploughing occurs and side flow of material is increased considerably. Although other factors may influence this critical rake angle in addition to the adhesion coefficient, the fact that a critical rake angle exists under some real cutting conditions supports the solution obtained here.

By holding the rake angle constant and varying the adhesion coefficient it was found that both cutting force components are lower when the friction is higher. When the adhesion coefficient is decreased, the cutting forces increase. For negative rake angles less than the maximum negative rake angle obtained in the frictionless case, approximately 71.6°, the adhesion coefficient can be decreased all the way to zero. As shown in

Figure 23, α_{max} decreases as the adhesion coefficient decreases. Thus for a given negative rake angle greater than 71.6^{o}, the adhesion coefficient can only be decreased until α_{max} becomes equal to the given rake angle. This means that at rake angles greater than the maximum allowable negative rake angle for the frictionless case, there is a minimum amount of friction required which must be present before cutting can occur.

This result suggests that the role of friction is very important in negative rake cutting, and at a given rake angle, the least cutting force is required when friction is highest. Intuitively this result seems correct since a negative rake tool cuts with a pushing action as opposed to the slicing action of a positive rake tool, and with a high frictional shear stress τ_2, the material is less likely to slide back under the tool and more likely to be pushed out to form a chip. The other shear stress, τ_1, opposes chip formation. However τ_1 is always much smaller in magnitude than τ_2 since the normal stress adjacent to the stress free chip is much lower than the normal stress on the lower section of the tool. Thus τ_2 is the dominant shear stress and increasing it decreases the required cutting force.

The cutting force increases rapidly as the rake angle approaches the critical rake angle for a given friction condition. In the limit, at the critical rake angle, no chip will form for any applied force. In a real cutting situation this means that increased force would cause an increase in side flow of the material but no chip formation. Figure 3 of Komanduri [11] shows the variation of experimentally measured cutting force components with rake angle for one set of cutting conditions. The experimentally determined curves are similar in shape to the theoretical curves of Figure 27 with the normal force component being larger and increasing

more rapidly than the tangential component. Thus in a general sense the theoretical results obtained here are comparable to experimental results although no attempt has been made here to simulate the experimental tests.

Very little experimental data is available for negative rake cutting. However, to enhance this work, it would be desireable to simulate some experimental tests with the theoretical solution obtained here and compare the numerical results.

Further work also needs to be done on this solution to clear up the pressure mis-match caused by the stress discontinuity FG. Knowledge about this type of stress discontinuity appears to be limited and possibly the only way to avoid the pressure mis-match is to resort to numerical methods to obtain a new slip-line field.

REFERENCES

1. Merchant, M. E., "Basic Mechanics of the Metal Cutting Process," Jour. Appl. Mech., 15, 1944, A-168.

2. _____, "Mechanics of the Metal Cutting Process-I: Orthogonal Cutting and the Type 2 Chip," Jour. Appl. Phys., 16, 1945, 267.

3. _____, "Mechanics of the Metal Cutting Process-II: Plasticity Conditions in Orthogonal Cutting," Jour. Appl. Phys., 16, 1945, 318.

4. Albrecht, P., "New Developments in the Theory of the Metal-Cutting Process, Part I: The Ploughing Process in Metal Cutting," Jour. Eng. Ind., Nov., 1960, 348.

5. Shaw, M. C., "A New Theory of Grinding," Mech. and Chem. Eng. Trans. of Inst. of Engrs., Australia, V. MC8, May 1972, 73.

6. Appl, F. C. and Rowley, D. S., "Analysis of the Cutting Action of a Single Diamond," Jour. Soc. Pet. Eng., September, 1968.

7. Rowley, D. S. and Appl, F. C., "Analysis of Surface Set Diamond Bit Performance," Jour Soc. Pet. Eng., September, 1969.

8. Rubenstein, C., Groszman, F. K., and Koenigsberger, F., "Force Measurements During Cutting Tests and Single Point Tools Simulating the Action of a Single Abrasive Grit," Science and Technology of Industrial Diamonds, 1967, Proc. Int. Indust. Dia. Conf., Oxford, 1966.

9. Connolly, R. and Rubenstein, C., "The Mechanics of Continuous Chip Formation in Orthogonal Cutting," Int. Jour. Mach. Tool Des. Res., V. 8, 1968, 159.

10. Rowe, G. W. and Wetton, A. G., "Theoretical Considerations in the Grinding of Metals," Jour. Inst. Metals, V. 97, 1969, 193.

11. Komanduri, R., "Some Aspects of Machining with Negative Rake Tools Simulating Grinding," Int. Jour. Mach. Tool Des. Res., Vol. 11, 1971, 223.

12. Lal, G. K. and Shaw, M. C., "Experiments with Spherical Tools," Wear, V. 29, 1974, 153.

13. Abdelmoneim, M. ES. and Scrutton, R. F., "Tool Edge Roundness and Stable Build-Up Formation in Finish Machining," Jour. Eng. Ind., Nov., 1974, 1259.

14. Sakamoto, T. and Tsukizoe, T., "Friction and Prow Formation in a Scratch Process of Copper by a Diamond Cone," Wear, V. 44, 1977, 393.

15. Basuray, P. K., Misra, B. K., and Lal, G. K., "Transition from Ploughing to Cutting During Machining with Blunt Tools," Wear, Vol. 43, 1977, 341.

16. Bitans, K. and Brown, R. H., "An Investigation in Orthogonal Cutting," Int. Jour. Mach. Tool Des. Res., Vol. 5, 1965, 155.

17. Hill, R., The Mathematical Theory of Plasticity, Oxford: The Clarendon Press, 1950.

18. Thomsen, E. G. and Yang, C. T. and Kobayashi, S., Mechanics of Plastic Deformation in Metal Processing, New York: The Macmillan Company, 1965.

19. Black, P. H., Theory of Metal Cutting, New York: McGraw Hill Book Co., 1961.

20. Crandall, S. H., Engineering Analysis, New York: McGraw Hill Book Co., 1956.

21. Johnson, W. and Sowerby, R., Plane-Strain Slip-Line Fields: Theory and Bibliography, New York: American Elsevier Pub. Co., 1970.

22. Wanheim, T., Bay, N. and Peterson, A. S., "A Theoretically Determined Model for Friction in Metal Work Processes," Wear, V. 28, 1974, 251.

23. Bowden, F. P. and Tabor, D, The Friction and Lubrication of Solids, London: The Oxford University Press, 1950.

APPENDIX A

COMPUTER PROGRAM

BRIEF DESCRIPTION OF PROGRAM

The program was written to calculate dimensionless forces and stresses for a variety of adhesion coefficients and rake angles. The first loop in the program varies the adhesion coefficient m. The initial value of m, (M), the step size (DM), and the number of steps over which m is to be varied (NM), are given before the loop begins. The adhesion coefficient can be varied from zero to near I.0. However for m equal to 1.0 the cutting forces become infinite.

The friction angle η_1 is found by solving equation (60) by an iterative process. The iteration is continued until the difference between the left and right sides of equation (60) is less than 0.0001.

The next loop varies the negative rake angle α. Since α can only be in the interval between α_{min} and α_{max}, the program selects NALP equally spaced values of α within this interval. However since the forces become infinite when α is equal to α_{max}, the largest value of α used is 0.1° less than α_{max}.

At each value of α, the program solves equation (63) numerically for η_2 by the same procedure which is used for η_1. However since η_2 and θ are related, the program first calculates η_2 using an arbitrarily assumed value of θ equal to 30°. Then using the calculated value of η_2, a new value of θ is obtained from the next loop which minimizes the cutting forces with respect to θ. This process is continued until the change in θ is less than 0.01°. Then the numerical results are printed out and α is incremented. When α has been incremented through its entire range, the adhesion coefficient is incremented and all the iterations are performed again.

PROGRAM LISTING

```
$JOB
   75 FORMAT(' ','M =',F6.3)
   89 FORMAT('-',10X,'DID NOT CONVERGE')
  101 FORMAT(' ',10X,10F10.3)
      REAL MU1,MU2,M
      PIO4=ATAN(1.0)
      RADDEG=45.0/PIO4
      DEGRAD=PIO4/45.0
      TTHSTO=10.0
      NALP=5
      ADIV=NALP-1
      RT2=SQRT(2.0)
      PIO2=2.0*PIO4
      EPS=0.0001
      M=0.5
      DM=0.1
      NM=2
C *** LOOP FOR VARYING THE ADHESION COEFFICIENT M ***
      DO 1 JJ=1,NM
      WRITE(6,75) M
      ARLIM=1.0-0.52*((1.0-M)**0.325)
      RHO=0.5*ARCOS(M)
      TRHO=2.0*RHO
      SIGNLM=RT2*(1.0+PIO2+TRHO+SIN(TRHO))/(2.0*RT2+4.0*SIN(RHO))
      MU1=0.5*M*ARLIM/SIGNLM
      BETA2=ARLIM/(1.0-ARLIM)/SIGNLM
      BETA1=(1.0-ARLIM)*EXP(BETA2*SIGNLM)
      DE1=10.0*DEGRAD
      TETA1=2.0*PIO4
C *** ITERATION FOR ETA 1 ***
      IITER=0
  210 ITER=0
  211 ELTEST=MU1*(1.0+SIN(TETA1))-COS(TETA1)
      IF(ELTEST.LT.0.0) GO TO 222
      TELSAV=TETA1
      TETA1=TETA1-DE1
      ITER=ITER+1
      IF(ITER.GT.12) GO TO 77
      GO TO 211
  222 IITER=IITER+1
      IF(IITER.GT.19) GO TO 900
      DIFF=TELSAV-TETA1
      IF(ABS(ELTEST).LT.EPS) GO TO 900
      DE1=DIFF*0.1
      TETA1=TELSAV
      GO TO 210
   77 WRITE(6,89)
  900 ETD=TELSAV*RADDEG
      ETA1=TETA1*0.5
      SIG1=1.0+SIN(TETA1)
      TAU1=COS(TETA1)
      TTH=60.0*DEGRAD
C *** LOOP FOR VARYING THE NEGATIVE RAKE ANGLE ALP          ***
      DO 600 JALP=1,NALP
      DELALP=(JALP-1)/ADIV
C *** BEGIN ITERATION FOR ETA 2 ***
      JITER=0
  310 DE2=10.0*DEGRAD
      TETA2=2.0*PIO4
      ETA2=0.5*TETA2
```

```
      IITER=0
  312 ITER=0
  311 E2TEST=M*(1.0-BETA1*EXP(-0.5*BETA2*(1.0+2.0*(TTH+ETA1+ETA2-PI02)+
     12.0*SIN(TTH)+SIN(TETA2))))-COS(TETA2)
      IF(E2TEST.LT.0.0) GO TO 322
      TE2SAV=TETA2
      TETA2=TETA2-DE2
      ITER=ITER+1
      IF(ITER.GT.12) GO TO 377
      GO TO 311
  322 IITER=IITER+1
      IF(IITER.GT.19) GO TO 300
      DIFF=TE2SAV-TETA2
      IF(ABS(E2TEST).LT.EPS) GO TO 300
      DE2=DIFF*0.1
      TETA2=TE2SAV
      GO TO 312
  377 WRITE(6,89)
  300 E2D=TE2SAV*RADDEG
      ETA2=TETA2*0.5
      ETA145=ETA1+PI04
      TTHMAX=PIC2
      TTHDIV=50.0
      NTH=TTHDIV
      AMAX=ATAN(TAN(ETA1)+1.0/SIN(ETA2)/COS(ETA1))
      AMIN=PI02-ETA2
      ALP=(AMAX-AMIN)*DELALP+AMIN
      IF(ALP.GE.AMAX) ALP=AMAX-0.1*DEGRAD
      ALPD=ALP*45.0/PI04
      CSE=COS(ALP)/SIN(ETA2)
      IF(CSE.GT.1.0) CSE=1.0
      ELCK=ALP-ARSIN(CSE)
      IF(ELCK.GT.ETA1) GO TO 600
      ALET1=ALP-ETA1
      TTHMIN=ARSIN(SIN(ETA2)*SIN(ALET1)/COS(ALP))
      DTTH=(TTHMAX-TTHMIN)/TTHDIV
      TTH=TTHMIN+DTTH
      TAU2=COS(TETA2)
      DL2=1.0/SIN(ETA2)
C *** LOOP TO MINIMIZE FORCES WITH RESPECT TO THETA ***
      DO 500 I=1,NTH
      SIG2=1.0+2.0*(TTH+ETA1+ETA2-PI02)+2.0*SIN(TTH)+SIN(TETA2)
      DL1=1.0/(RT2*SIN(TTH)*SIN(ETA145))
      PRES=SIG1*DL1+SIG2*DL2
      TAUS=TAU2*DL2-TAU1*DL1
      TOLEN=DL1+DL2
      T=COS(ALP)/SIN(ETA2)-SIN(ALET1)/SIN(TTH)
      PAVG=PRES/TOLEN
      FT=(PRES*COS(ALP)+TALS*SIN(ALP))/T
      FN=(PRES*SIN(ALP)-TAUS*COS(ALP))/T
      THD=TTH*45.0/PIO2
      IF(I.EQ.1) GO TO 499
      IF(FTSAVE.LT.FT) GO TO 450
      IF(I.EQ.NTH) GO TO 451
      GO TO 499
  450 THD=(TTH-DTTH)*45.0/PIC2
      GO TO 550
  451 THD=TTH*45.0/PIO2
  499 TTH=TTH+DTTH
      FTSAVE=FT
```

```
      FNSAVE=FN
      PAVGSV=PAVG
      TSAVE=T
  500 CONTINUE
      TTH=THO*2.0*DEGRAD
  550 CONTINUE
      JITER=JITER+1
      IF(JITER.GT.9) GO TO 899
      CHECK=TTH-TTHSTO
      CHECKD=CHECK*RADDEG
      IF(ABS(CHECK).LT.0.00034) GO TO 999
      TTHSTO=TTH
      GO TO 310
C *** END ITERATION FOR ETA2 ***
  899 WRITE(6,85)
  999 CONTINUE
      AMAXD=AMAX*RADDEG
      AMIND=AMIN*RADDEG
      WRITE(6,101) ALPO,TAU1,SIG1,TAU2,SIG2,FTSAVE,FNSAVE,PAVGSV,THO,T
  600 CONTINUE
      M=M+DM
    1 CONTINUE
      STOP
      END
$ENTRY
```

APPENDIX B

NUMERICAL RESULTS

TABLE II

NUMERICAL RESULTS

m	α (Degrees)	$\frac{\tau_1}{k}$	$\frac{\sigma_1}{k}$	$\frac{\tau_2}{k}$	$\frac{\sigma_2}{k}$	$\frac{F_t}{tk}$	$\frac{F_n}{tk}$	$\frac{P_m}{k}$	θ (Degrees)
0.500	58.515	0.220	1.975	0.454	4.979	10.6	15.2	4.010	28.870
	62.414	0.220	1.975	0.466	5.490	13.4	22.3	4.451	34.245
	66.100	0.220	1.975	0.472	5.895	18.5	36.0	4.796	39.034
	69.664	0.220	1.975	0.476	6.156	33.2	75.9	5.015	42.562
	73.068	0.220	1.975	0.478	6.300	1007.0	2740.1	5.143	44.926
0.600	62.210	0.274	1.962	0.565	5.172	12.5	19.7	4.272	33.331
	65.311	0.274	1.962	0.572	5.526	15.7	28.2	4.579	37.413
	68.266	0.274	1.962	0.576	5.769	21.9	44.7	4.789	40.512
	71.156	0.274	1.962	0.579	5.956	39.8	93.3	4.948	43.143
	78.901	0.274	1.962	0.580	6.060	1004.3	2717.3	5.045	44.925
0.700	66.245	0.334	1.942	0.675	5.190	15.2	26.9	4.397	36.742
	68.554	0.334	1.942	0.679	5.385	19.2	37.6	4.570	39.174
	70.819	0.334	1.942	0.681	5.585	27.0	58.8	4.744	41.849
	73.025	0.334	1.942	0.683	5.708	50.0	121.5	4.852	43.666
	75.103	0.334	1.942	0.684	5.777	988.7	2685.3	4.922	44.924
0.800	70.900	0.402	1.916	0.786	5.087	19.9	40.3	4.438	39.775
	72.457	0.402	1.916	0.787	5.197	25.3	55.4	4.537	41.263
	73.993	0.402	1.916	0.788	5.292	36.1	85.3	4.624	42.631
	75.513	0.402	1.916	0.789	5.391	68.1	174.8	4.714	44.130
	76.908	0.402	1.916	0.790	5.431	951.5	2637.1	4.759	44.921

TABLE II (Continued)

m	α (Degrees)	$\frac{\tau_1}{k}$	$\frac{\sigma_1}{k}$	$\frac{\tau_2}{k}$	$\frac{\sigma_2}{k}$	$\frac{F_t}{tk}$	$\frac{F_n}{tk}$	$\frac{Pm}{k}$	θ (Degrees)
0.900	76.775	0.484	1.875	0.895	4.814	31.2	76.0	4.363	42.375
	77.591	0.484	1.875	0.896	4.860	40.3	102.8	4.407	43.057
	78.405	0.484	1.875	0.896	4.901	58.5	156.4	4.448	43.696
	79.217	0.484	1.875	0.896	4.953	113.0	317.2	4.499	44.525
	79.919	0.484	1.875	0.896	4.969	872.9	2554.1	4.522	44.913
0.999	88.750	0.646	1.764	0.999	3.956	481.5	1767.2	3.903	44.738
	88.777	0.646	1.764	0.999	3.956	608.8	2247.9	3.921	44.999
	88.782	0.646	1.764	0.999	3.956	640.4	2365.4	3.921	44.999
	88.813	0.646	1.764	0.999	3.956	958.5	3548.2	3.921	44.999
	88.845	0.646	1.764	0.999	3.956	1912.2	7094.3	3.921	44.999

ACKNOWLEDGEMENTS

I wish to express my sincere appreciation to Dr. F. C. Appl for his direction and consultation. Thanks are also due to Christensen Diamond Products Company for their financial support of this project.

I would further like to thank my wife, Susan, for her help with the drawings, and for her faithful support and encouragement throughout my graduate study.

VITA

JOHN WAYNE HEIN

Candidate for the Degree

Master of Science

THESIS: THEORETICAL ANALYSIS OF METAL CUTTING WITH LARGE NEGATIVE RAKE CUTTING TOOLS

MAJOR FIELD: Mechanical Engineering

BIOGRAPHICAL:

Personal Data: Born March 9, 1955 at Hutchinson, Kansas; the son of John J. and Darlean M. Hein.

Education: Graduated from Buhler High School, Buhler, Kansas in 1973; attended Hutchinson Community Junior College until 1975; received a B.S. degree in Mechanical Engineering from Kansas State University in 1977; completed requirements for the M.S. degree in February, 1979.

THEORETICAL ANALYSIS OF METAL CUTTING WITH LARGE NEGATIVE RAKE CUTTING TOOLS

by

JOHN WAYNE HEIN

B.S., Kansas State University, 1977

AN ABSTRACT OF

A MASTER'S THESIS

Submitted in Partial Fulfillment of the

Requirements for the Degree

MASTER OF SCIENCE

Department of Mechanical Engineering

Kansas State University

Manhattan, Kansas

1979

ABSTRACT

An approximate slip-line field is developed for a range of negative rake angles beyond the range where ordinary metal cutting theory applies. In this range of large negative rake angles, the flow of metal along the tool is in opposite directions on either side of a stagnation point on the tool. This divided flow results in frictional stresses which are also in opposite directions. The slip-line field accounts for this complex friction distribution and is used to calculate the cutting forces and frictional stresses for various rake angles and friction coefficients.